Mouse model of intrahepatic cholangiocarcinoma validates FIG–ROS as a potent fusion oncogene and therapeutic target

Anna Saborowski[a,b,1], Michael Saborowski[a,b,1], Monika A. Davare[c], Brian J. Druker[c,d], David S. Klimstra[e], and Scott W. Lowe[a,b,d,2]

[a]Cancer Biology and Genetics Program and [e]Department of Pathology, Memorial Sloan–Kettering Cancer Center, New York, NY 10065; [b]Cold Spring Harbor Laboratory, Cold Spring Harbor, NY 11724; [d]Howard Hughes Medical Institute; and [c]Knight Cancer Institute, Oregon Health and Science University, Portland, OR 97239

Cholangiocarcinoma is the second most common primary liver cancer and responds poorly to existing therapies. Intrahepatic cholangiocarcinoma (ICC) likely originates from the biliary tree and develops within the hepatic parenchyma. We have generated a flexible orthotopic allograft mouse model of ICC that incorporates common genetic alterations identified in human ICC and histologically resembles the human disease. We examined the utility of this model to validate driver alterations in ICC and tested their suitability as therapeutic targets. Specifically, we showed that the fused-in-glioblastoma-c-ros-oncogene1 (FIG–ROS1(S); FIG–ROS) fusion gene dramatically accelerates ICC development and that its inactivation in established tumors has a potent antitumor effect. Our studies establish a versatile model of ICC that will be a useful preclinical tool and validate ROS1 fusions as potent oncoproteins and therapeutic targets in ICC and potentially other tumor types.

Cholangiocarcinoma, the second most common primary liver cancer, has a dismal prognosis due to its poor responsiveness to existing therapies. It represents 10–25% of primary liver cancers worldwide (1), but is more frequent in Asia, due to a higher prevalence of risk factors such as parasitic infections, biliary-duct cysts, hepatolithiasis, and primary sclerosing cholangitis (2). Intrahepatic cholangiocarcinoma (ICC) develops within the liver parenchyma, shows markers of cholangiocyte differentiation, including positivity for cytokeratin 19, and leads to abundant stromal desmoplasia. Whereas surgical resection can be curative, most patients are not eligible for this procedure due to advanced disease, and no effective systemic therapy has been developed to date (3, 4).

Sequencing efforts are beginning to generate in-depth information about the somatic alterations that occur in cholangiocarcinoma. Among the most frequently mutated genes are the tumor suppressor tumor protein p53 (TP53) (37–44%) (5, 6) and the kirsten rat sarcoma viral oncogene homolog (KRAS) (17–54%) (6–8), although mutations in MLL3 and SMAD4 are also common (15% and 17% of cases, respectively) (6). Despite their high mutational frequency, none of these signature genes is amenable to targeted therapy.

Recently, the mutational spectrum of cholangiocarcinoma has been extended by the identification of ROS1 fusions in nearly 9% of cholangiocarcinoma patients (9). Oncogenic fusion kinases involving the orphan receptor tyrosine kinase ROS1 have been previously reported at low frequency in lung adenocarcinoma and glioblastoma and result from chromosomal rearrangements that lead to constitutive activation of the ROS1 kinase activity. Consequently, ROS1 presents a potential drug target for a subset of patients with ICC.

Mouse models have proven a powerful tool for understanding the relationship between cancer genetics and tumor behavior, but only a few genetically engineered mouse models (GEMMs) of ICC exist and many display a mixed ICC/hepatocellular carcinoma

(HCC) histology (10–13). A histopathologically accurate ICC model has been produced by liver-specific expression of endogenous KrasG12D mutant in combination with Tp53 tumor suppressor gene deletion (14). Still, as with other multiallelic GEMMs, this model requires time-consuming and expensive breeding strategies to integrate further genetic changes. Moreover, because the conditional alleles cause the alteration to be present throughout the entire organ, the majority of GEMMs do not recapitulate the human microenvironment where cancer cells and normal cells are both present and interact. Faster and more flexible in vivo models would greatly facilitate the functional characterization of candidate driver alterations and therapeutic targets, as well as produce tractable preclinical models for testing novel therapies.

Our laboratory has previously established an orthotopic allograft mouse model for hepatocellular carcinoma that is based on the genetic manipulation of liver progenitor cells followed by the orthotopic transplantation into recipient mice (15, 16). This model enabled us to rapidly study genetic interactions during tumorigenesis as well as to identify and functionally validate tumor suppressor genes and oncogenes. Here we describe the development of a similar model for ICC that allows

Significance

Intrahepatic cholangiocarcinoma (ICC) is a fatal yet understudied primary liver malignancy. To accelerate the functional annotation of cancer genes and therapeutic targets in this disease, we generate a highly flexible orthotopic allograft mouse model of ICC that can be easily modified in vitro to mimic either oncogene expression by retrovirus-mediated gene transfer or tumor-suppressor gene loss by using RNA interference technology. We use this model to demonstrate that the fused-in-glioblastoma-c-ros-oncogene 1 (FIG-ROS) fusion, which is found in a subset of ICC patients, accelerates cholangiocarcinogenesis. Moreover, by using reversible gene expression, we show that FIG–ROS inactivation in carcinomas harboring mutant kirsten rat sarcoma viral oncogene homolog (Kras) and p53 mutations can potently inhibit tumor growth, thereby validating ROS as a therapeutic target in ICC.

MEDICAL SCIENCES

us to rapidly interrogate biologically relevant aspects of this disease. We use this system to functionally validate FIG–ROS as a potent oncoprotein in ICC and document its requirement for tumor maintenance, thus confirming its potential as a therapeutic target.

Results

Differential Effects of c-Myc and Kras on Tumors Initiated from Liver Progenitor Cells.

Our previous progenitor-cell–based mouse model of liver cancer involved the isolation and the retroviral transduction of E-cadherin positive fetal liver cells from $p53^{-/-}$ embryos with different oncogenes, followed by transplantation of the genetically modified cell populations into recipient mice. In an attempt to improve this model, we used a strategy to incorporate conditional mutant alleles exclusively in the hepatic parenchymal cells. Specifically, we generated mice harboring an *Albumin-Cre* (*Alb-Cre*) transgene together with two different conditional mutant *p53* alleles (*p53^lox^* and *p53^lslR172H^*, designated *p53^lslR172H/lox^*) (17, 18) (Fig. 1A). As Alb-Cre is a liver-specific Cre-recombinase expressed in bipotent liver progenitor cells and adult hepatocytes (19–21), its expression in the *p53^lslR172H/lox^* background produces liver-specific expression of a mutant *p53* and deletion of the other allele, which is a typical configuration occurring in human tumors.

Initially, to test whether oncogenes known to cooperate with *p53* mutations would produce liver carcinomas in this model, we transduced fetal liver cells isolated from *Alb-Cre; p53^lslR172H/lox^* embryos (subsequently referred to as AP cells) with retroviral vectors coexpressing green fluorescent protein (GFP) with either v-myc myelocytomatosis viral oncogene homolog (c-Myc) or Kras^G12D^. Following intrahepatic injection of the resulting cell populations, recipient mice rapidly developed tumors with complete penetrance (Fig. 1C).

Surprisingly, the histopathology of tumors triggered by expression of c-Myc and oncogenic Ras was distinct. Consistent with previous work (15, 16), tumors induced by c-Myc resembled human HCC, corroborated by strong nuclear expression of hepatic nuclear factor 4 alpha (HNF4A) and a granular, cytoplasmic reactivity with anti-hepatocyte paraffin-1 (Hep Par1), an antibody frequently used in the clinical diagnosis of HCC (Fig. 1E); conversely, they were negative for cytokeratin 19 (CK19), a marker for ductal differentiation. The histological spectrum of resulting HCCs ranked from pseudoglandular to solid carcinomas (Fig. S1). In contrast, tumors induced by Kras^G12D^ presented as a gland-forming adenocarcinoma. As is observed in human ICC, malignant epithelial cells were surrounded by a marked stromal desmoplasia that was not observed in tumors overexpressing c-Myc (Fig. 1 D and E). Although this stromal reaction was triggered by the transplanted cells, it was derived from the host, as the stromal cells did not stain for the transduced GFP reporter. These results are consistent with the frequent occurrence of *KRAS* mutations in human ICC (6, 8) and their relative infrequent occurrence in HCC (22) and indicate that oncogenic Kras biases the malignant fate of transduced cell populations to ICC.

Development of an Orthotopic Allograft Model of ICC.

The observations above and previous work suggested that it would be possible to produce an orthotopic allograft mouse model of ICC from liver progenitor cells simply incorporating mutant *Kras* instead of *c-Myc*. To achieve this and to eliminate the potential nonphysiological consequences of Kras overexpression, we introduced a cre-activatable endogenous *Kras^G12D^* allele (*Kras^lslG12D^*) into our base configuration (23). Next, isolated liver progenitor cells of the genotype *Alb-Cre; Kras^lslG12D^; p53^lslR172H/lox^* (subsequently referred to as AKP cells) were transduced with a GFP reporter and transplanted intrahepatically into recipient mice. The recipient animals succumbed to liver cancers with a median survival of 84 d, significantly longer than mice transplanted with AP cells overexpressing Kras^G12D^ (Fig. 1C, $P = 0.045$). In contrast, mice receiving AP cells transduced with a control plasmid did not develop liver tumors within 9 mo of follow-up. Thus, consistent with observations from strictly germ-line systems (14), endogenous *Kras^G12D^* cooperated with *p53* mutations in our model.

Beyond large tumors in the liver, moribund animals harboring Kras^G12D^/mutant p53 tumors often displayed hemorrhagic ascites and/or breathing failure due to metastatic disease to the lung (Fig. S2). Histologically, the GFP-expressing tumor cells were embedded in a GFP-negative and thus recipient-derived stroma rich in collagen fibers [Fig. 2A, GFP immunohistochemistry (IHC) and Masson's trichrome stain]. Flow cytometry revealed that when gated on the CD45 negative population, only 17–22% of all cells were GFP positive, illustrating the abundance of

Fig. 1. Development of genetically defined, oncogene-dependent orthotopic allograft models of liver cancer. (*A*) Technical outline. ED14.5 fetal liver cells from *Alb-Cre; p53^lslR172H/flox^* (AP) or *Alb-Cre; Kras^lslG12D^; p53^lslR172H/flox^* (AKP) embryos are enzymatically isolated and expanded in culture. After transduction with MSCV-based retroviruses coencoding a fluorescent marker and an oncogene or shRNAs directed against tumor suppressor genes, cells were orthotopically transplanted into the livers of recipient mice. (*B*) Brightfield and fluorescent images of orthotopic tumors derived from AP cells expressing retrovirally introduced and GFP-linked Kras^G12D^ or c-Myc. (*C*) Kaplan–Meier survival curves of recipient animals transplanted with Kras^G12D^ or c-Myc overexpressing AP cells, AKP cells, or AP cells transduced with a control retrovirus expressing turbo RFP. $n \geq 4$. (*D*) AP cells overexpressing Kras^G12D^ give rise to tumors that histologically resemble moderately differentiated and CK19 positive cholangiocarcinoma. GFP expression identifies cancer cells that originate from transplanted AP cells within the recipient-derived GFP negative stroma. (Scale bars, 25 μm.) (*E*) c-Myc overexpression in AP cells leads to HCC formation. Strong nuclear staining for HNF4a indicates that tumor cells retain features of hepatocyte differentiation (*Upper*, normal liver; *Lower*, tumor). CK19 is expressed in normal bile duct cells within the liver (*Upper*) but not in the tumor cells (*Lower*). Granular, cytoplasmic staining pattern indicates positivity for HepPar1. (Scale bars, 25 μm, unless otherwise indicated.)
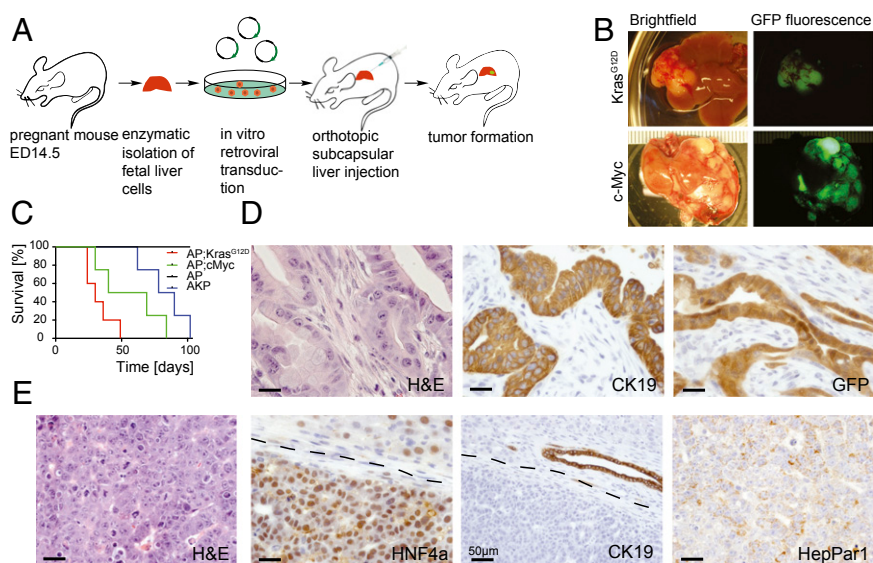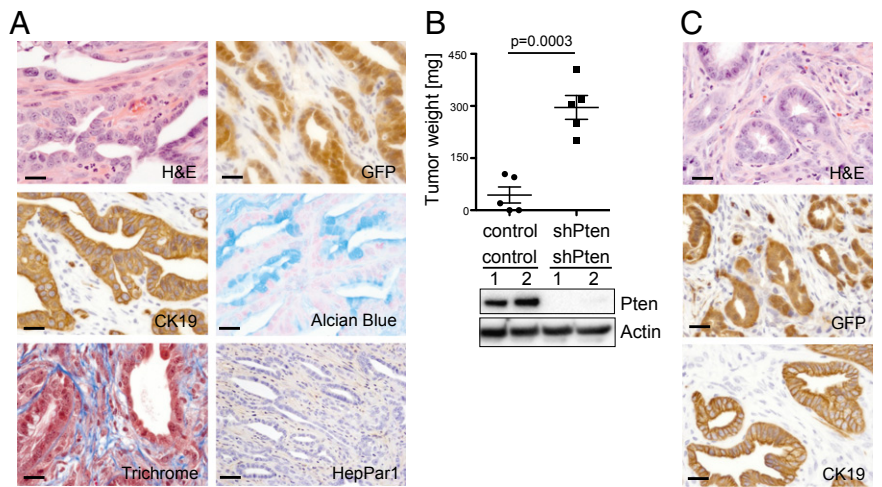
Fig. 2. The AKP hepatoblast transplantation model gives rise to tumors that resemble primary human ICC and enables functional validation of oncogenic drivers. (*A*) Histopathology of tumors generated by orthotopic injection of GFP-transduced AKP cells. H&E reveals gland-forming epithelial cancer cells that express the ductal differentiation marker CK19. GFP IHC distinguishes between GFP-positive cancer cells derived from the transplanted cells and recipient-derived GFP-negative desmoplastic stroma rich in collagen fibers (dark blue in Masson's trichrome stain). Mucin-producing cells in well-differentiated areas appear as dark blue in the Alcian Blue stain. (Scale bars, 25 μm.) (*B*) Tumor burden is increased by RNAi-mediated knockdown of the tumor suppressor Pten. Mice were injected with AKP cells transduced with either a control hairpin (shRenilla) or a potent shRNA targeting Pten (shPten) and euthanized 5 wk after transplantation. Efficient Pten knockdown is confirmed by immunoblot on GFP sorted cells from shPten tumors. (*C*) AKP cells transduced with shPten lead to CK19 positive, moderately differentiated ICC. (Scale bars, 25 μm.)

stroma within the tumors ([Fig. S3](#)). The epithelial tumor cells stained positive for CK19, a marker of ductal differentiation (Fig. 2*A*), and were in part mucin producing [confirmed by Alcian Blue stain (Fig. 2*A*)]. Finally, the tumors were negative for HepPar1 (Fig. 2*A*), confirming they were not hepatocellular carcinoma. Overall, the model closely recapitulates histologic hallmark features of moderately differentiated cholangiocarcinoma in humans.

To determine whether perturbing an established cancer pathway might further alter the observed tumor phenotypes, we also transduced parallel populations with vectors expressing short-hairpin RNAs (shRNAs) targeting Pten (shPten) or a neutral control (shRenilla). Of note, the Pten shRNA potently suppresses target gene expression by RNA interference (24), thereby deregulating the PI3K pathway and mimicking genetic changes that occur in ICC and many other cancer types (25). Five weeks posttransplantation, recipient mice that had received Pten-suppressed AKP cells presented with a significantly increased tumor burden compared with mice transplanted with control transduced cells (Fig. 2*B*). Importantly, whereas Pten suppression accelerated tumor growth compared with a control shRNA, it did not substantially alter the histology of resulting tumors (Fig. 2*C*). These results illustrate the potential of the system to study cancer drivers while maintaining an accurate histology and, further, how shRNA technology can be incorporated to study loss-of-function phenotypes. Of note, experiments to document interactions between oncogenic Kras, mutant p53, and Pten inactivation using strictly germ-line strains would have required the intercrossing of six mutant alleles.

FIG–ROS Is a Potent Driver in Cholangiocarcinogenesis. The above data provide evidence that our ICC model will facilitate the in vivo validation of candidate driver genes identified through genomic studies without the time and cost of producing new transgenic or knockout strains. To examine a functionally uncharacterized lesion in this system, we chose to study the FIG–ROS fusion protein as a potential cancer driver and therapeutic target in ICC. Murine stem cell virus (MSCV)-based retroviruses encoding a FIG–ROS cDNA linked to GFP or a control vector expressing turboRFP (pMSCV-turboRFP-IRES-GFP) were transduced into fetal AP or AKP liver cells. The resulting cell populations were orthotopically transplanted into recipient mice, which were monitored for tumor onset and pathology. In the presence of Kras^{G12D} and mutant p53, FIG–ROS markedly accelerated tumor growth relative to control tRFP-expressing tumors (Fig. 3*B*), with a median survival of 32 d and 79 d, respectively (Fig. 3*C*, $P < 0.0001$). Interestingly, in the

absence of Kras^{G12D}, FIG–ROS was still able to promote tumorigenesis, but at a reduced penetrance and longer latency (Fig. 3*C*).

Gross pathology of moribund mice identified large tumors in the liver and frequent lung metastases. Expression of FIG–ROS in the resulting tumors was indicated by GFP fluorescence and further confirmed by ROS1 immunohistochemistry on tumor sections (Fig. 4*A*). Histologically, FIG–ROS-expressing tumors derived from AKP cells presented as cholangiocarcinoma, albeit with increased areas of poor differentiation (Fig. 4*A*). Accordingly, CK19 expression remained positive and stromal desmoplasia was present. By marked contrast, all three tumors that arose in the absence of mutant Kras resembled HCC, confirmed by the presence and absence of HNF4α- and CK19 staining, respectively. These observations underscore the plasticity of the fetal liver-cell–based system and the linkage between tumor histopathology and driving genetic events (Fig. 4*D*).

ROS triggers the phosphorylation of Shp2 and other effector proteins and exerts its function through multiple effectors, including components of the Jak/Stat, MAPK, and PI3K pathways (26). Accordingly, tumor cell lines established from FIG–ROS-expressing tumors showed up-regulation of known ROS1 effectors such as pShp2 and pStat3 by immunoblotting, compared with control cell lines established from either tRFP- or shPten-expressing tumors (Fig. 4*C*). pAkt levels were elevated in both the FIG–ROS and the shPten cell lines, as expected. These cells rapidly formed lethal tumors that, at low passage, retained the histopathology of ICC upon retransplantation into recipient mice (Fig. 4*B*). These observations confirm that the primary ICCs were indeed malignant and establish panels of genetically characterized tumors that can be used for preclinical studies to assess candidate ICC therapeutics.

FIG–ROS Is Required for the Maintenance of ICC. Owing to their deregulated tyrosine kinase activity, ROS1 fusion oncoproteins represent potential therapeutic targets. Still, all ROS inhibitors identified to date target multiple kinases and are insufficient tools to demonstrate that ROS activity is required for tumor maintenance. To examine this question in ICC, we used the tetracycline-based conditional expression system to ask whether inhibition of FIG–ROS in established cancers would have an anticancer effect. Adapting the approach shown in Fig. 5*A*, we generated a retrovirus that constitutively expresses mCherry to track transduced cells and the FIG–ROS cDNA linked to a GFP reporter under the control of a tet-responsive promoter. AKP cells were cotransduced with the doxycycline-inducible FIG–ROS
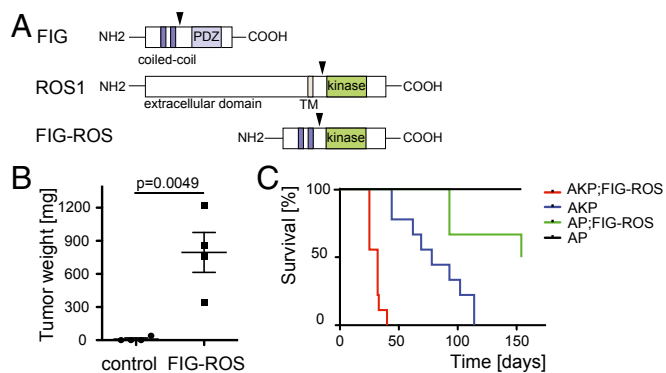
MEDICAL SCIENCES

Fig. 3. Expression of the FIG–ROS fusion accelerates hepatocarcinogenesis. (*A*) Schematic of the FIG–ROS1(S) fusion (here denoted as FIG–ROS) found in human cholangiocarcinoma, adapted from Gu et al. (9). (*B*) Weight of explanted tumors 5 wk after intrahepatic injection of FIG–ROS or control (tRFP) transduced AKP cells. (*C*) Kaplan–Meier survival curve of mice orthotopically transplanted with AKP cells expressing FIG–ROS (red) or tRFP control (blue). In green: three of six mice that received FIG–ROS-transduced AP cells (but not control-transduced AP cells, black) developed tumors at longer latency. $n \geq 6$.

of the genetics and biology of this highly aggressive disease, we generated a genetically tractable mouse model of ICC that is based on the isolation and in vitro modification of fetal liver cells harboring *Kras* and *p53* mutations, two of the most common genetic alterations found in human ICC (6–8). We confirmed that tumors generated in this model closely resemble the histopathology of human ICC and display key characteristics like CK19 expression of the epithelial tumor cells and abundant stromal desmoplasia. We believe this is an important feature of
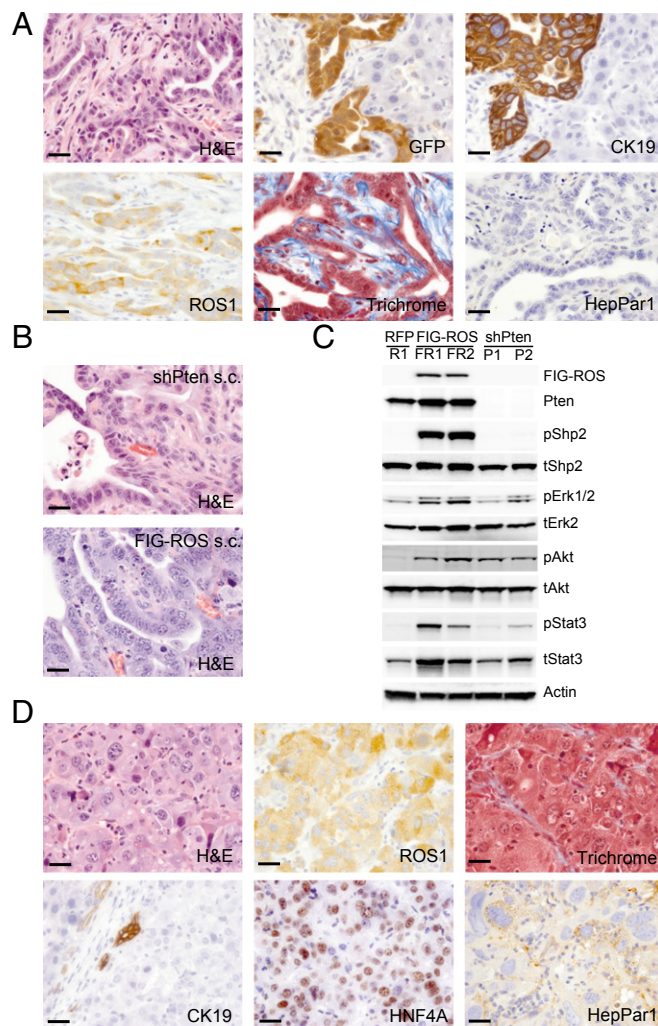

Fig. 4. FIG–ROS and Kras[G12D] cooperatively induce moderately differentiated ICCs in mice. (*A*) Histopathology of murine ICCs originating from FIG–ROS-expressing AKP cells retain hallmark features of cholangiocarcinoma. Gland-forming and CK19-positive tumor cells are surrounded by abundant stroma rich in collagen fibers (trichrome). ROS1 IHC confirms FIG–ROS expression in the tumor cells. Consistent with the majority of human ICCs, tumors lack positivity for HepPar1. (Scale bars, 25 μm.) (*B*) Cell lines derived from murine cholangiocarcinomas retain the histological characteristics of the parental tumors upon s.c. injection (H&E stains). Cell lines were established from AKP; shPten or AKP; FIG–ROS orthotopic tumors. (Scale bars, 25 μm.) (*C*) Immunoblot for key downstream signaling molecules comparing cell lines derived from tumors generated in the model and expressing either tRFP (one line), FIG–ROS (two lines, FR1 and FR2), or a potent shRNA directed against Pten (two lines, P1 and P2). (*D*) FIG–ROS-expressing AP cells lacking the *Kras[G12D]* allele lead to HCC development. These tumors exhibit significantly fewer collagen fibers than ICC counterparts (trichrome) and are negative for CK19 (normal bile duct as internal positive control). Strong positive nuclear expression of HNF4a and granular cytoplasmic staining pattern with HepPar1 further confirm the HCC phenotype. (Scale bars, 25 μm.)
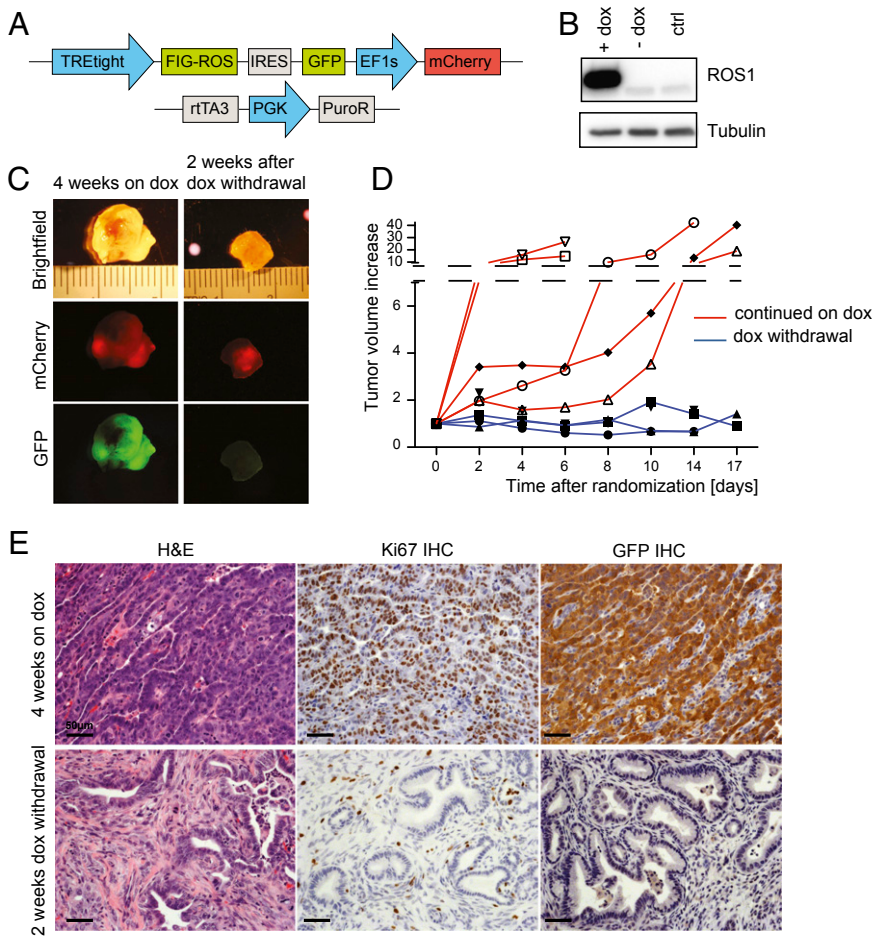
expression construct as well as a retroviral construct encoding for a reverse tet transactivator (rtTA$_3$) (pMSCV–rtTA$_3$–PGK–puromycin-resistance), enabling FIG–ROS expression to be reversibly induced by addition of the tetracycline analog, doxycycline (dox). Accordingly, dox-dependent expression of FIG–ROS was confirmed by immunoblotting (Fig. 5*B*).

Transduced cells were transplanted s.c. into recipient mice and the animals were placed on a dox-containing diet to enforce FIG–ROS expression. Successful engraftment of cells was confirmed by whole body fluorescence detection of the constitutively active red fluorescent reporter (mCherry) 10 d postinjection. Two weeks after implantation, all mice (nine of nine) on dox developed measurable tumors and were randomized into two treatment arms: five mice continued on dox, whereas the remaining mice were returned to regular mouse chow (off dox).

These experiments decisively established the importance of FIG–ROS for cancer maintenance. Hence, whereas tumors in mice maintained on dox grew rapidly, tumors from mice switched to an off-dox diet remained stable until 5 wk postimplantation (Fig. 5*D*). At this stage, masses derived from FIG–ROS-silenced tumors consisted of mostly cystic lesions harboring only small solid components that, histologically, were substantially less cellular than on-dox tumors and were dominated by the stromal compartment (Fig. 5*E*, H&E). Of note, a control group of mice that was continuously kept off dox after transplantation did not develop measurable tumors until 7 wk postinjection.

The primary cellular response to FIG–ROS withdrawal appeared to be cell-cycle arrest, as observed by the reduced Ki67 staining within the remaining epithelial tumor cells in the dox-withdrawal cohort compared with on-dox samples (Fig. 5*E*). Accordingly, FIG–ROS withdrawal in cultured tumor cells led to efficient down-regulation of ROS effector pathways accompanied by a reduction in colony formation in vitro (Fig. S4 *A*–*C*). The fact that these advanced ICCs remained "addicted" to FIG–ROS expression was particularly surprising, given these tumor cells also harbored *Kras* and *p53* mutations, and implies that human cholangiocarcinoma patients harboring the FIG–ROS fusion may greatly benefit from molecularly targeted therapy aimed at ROS1 fusions.

Discussion

Intrahepatic cholangiocarcinoma is a fatal yet understudied primary malignancy of the liver. To advance the understanding

Fig. 5. Doxycycline-regulated expression of FIG–ROS demonstrates its role in tumor progression and confirms the oncogenic fusion as a potent drug target. (*A*) Schematic of the tet-on vector system used for the reversible expression of FIG–ROS. TREtight-driven FIG–ROS expression linked to a GFP fluorescent reporter allows for the inducible, reversible expression of the oncogenic fusion. mCherry under a constitutive promoter serves as a marker of integration. The reverse tet-transactivator element (rtTA₃) is encoded on a separate vector due to size limitations. (*B*) Immunoblot of primary ED14.5 fetal liver cells cotransduced with the inducible FIG–ROS and the rtTA₃ expression construct confirming the expression of ROS1 only in the presence of doxycycline. Control: untransduced fetal liver cells. (*C*) Brightfield and fluorescent images of tumors derived from AKP cells transduced with the inducible FIG–ROS expression system. Recipient mice were either kept on dox food for 4 wk or changed to regular mouse chow 2 wk after injection. Efficient quiescence of GFP fluorescence in the off-dox tumor indicates termination of FIG–ROS expression. (*D*) Mice s.c. injected with primary AKP cells transduced with the inducible FIG–ROS system were kept on dox food for 14 d and then randomized to either continue on dox food or return to regular mouse chow. Tumor volume was followed by caliper measurements. FIG–ROS-expressing tumors grew rapidly, whereas tumor growth was abrogated in the dox-withdrawal cohort. (*E*) Representative histological images from on- versus off-dox tumors. On-dox tumors exhibit abundant actively proliferating cancer cells as assessed by Ki67 staining. Off-dox tumors are less cellular with more defined ductal structures and only a few Ki67-positive cells. GFP IHC: loss of GFP indicates effective termination of FIG–ROS expression. (Scale bars, 50 μm.)

the model as previous work from pancreas carcinoma—another glandular carcinoma also driven by *KRAS* mutations—indicates the stromal microenvironment has a major impact on cancer trajectory and treatment response (27).

Although recent advances in sequencing technologies have enabled in-depth characterization of the genomic landscape of human cancers, studies on the functional consequences of somatic mutations in cancer are necessary to understand the mechanistic impact of individual lesions and to identify candidate therapeutic approaches for targeting cancers of specific genotypes. The opportunity to genetically modify progenitor cells by retroviral gene transfer in vitro before transplantation allows for the rapid functional annotation of cancer genes and thus makes this mouse model much more flexible than those derived solely from germline alleles.

Beyond analysis of single genes, orthotopic allograft models enable in vivo pool-based screens for candidate oncogenes and tumor suppressor genes identified from genomic studies (28–30), and it seems likely that this ICC model will be highly amenable to this approach. Moreover, because genetic alterations are exclusively introduced into the epithelial cells but not in the recipient-derived stroma, the transplant approach may also serve as a valuable tool to investigate tumor–stroma interactions, with the fluorescent marker providing a convenient method to separate tumor and stromal compartments.

The Albumin-Cre used in our model becomes active in progenitor cells capable of differentiating into either the hepatocyte or bile duct lineage. Activation of *Kras^G12D* using Alb-Cre produces a ductal adenocarcinoma with all of the features of ICC. In line with previous reports (15), when these same progenitor-

enriched populations were transduced with c-Myc, the resulting tumors present as hepatocellular carcinoma. Apparently, *Kras* mutations predispose liver progenitor cells to ICC. Although the molecular basis underlying this observation remains unknown, the outcome is consistent with the observed incidence of these lesions in the human setting: increases in MYC copy number and/or expression are common in HCC, whereas activating mutations in *KRAS* are common in ICC. Of note, enforced expression of oncogenic Hras produces a mixed ICC/HCC model (31, 32), further underscoring the impact of initiating oncogenic lesions to impact the histopathology of liver malignancies.

Initially identified in a glioblastoma cell line (33, 34), translocations leading to the constitutive activation of ROS1 kinase have been observed in a variety of tumor types. Our results validate *FIG–ROS* as a potent oncogene in a mouse model of cholangiocarcinoma, where it potently cooperates with *Kras^G12D* and mutant *p53* to accelerate tumor onset, leading to an aggressive and metastatic disease. Interestingly, the ability of FIG–ROS to promote ICC was dependent on the presence of activated Kras, as FIG–ROS expression in its absence produced hepatocellular carcinoma at long latency and incomplete penetrance. These results are unexpected and suggest that, in ICC, signaling downstream of ROS1 complements but does not substitute for KRAS action. That FIG–ROS can drive HCC in the absence of oncogenic KRAS underscores the importance of KRAS in producing ductal carcinomas and suggests a broader but as yet undocumented role of ROS1 fusions in hepatobiliary malignancies.

Although *KRAS* and *TP53* mutations are among the most frequent genetic alterations in cholangiocarcinoma and other cancers, efforts to produce drugs targeting these mutations have

MEDICAL SCIENCES

proven unsuccessful. Our results imply that ROS1 inhibitors would be effective against a subset of human ICC harboring ROS1 fusion proteins. Although these events are relatively rare, small molecule inhibitors capable of inhibiting ROS1 kinase activity have been identified and are in clinical trials in lung cancer patients harboring tumors with ROS1 fusion events (35). As more druggable targets are identified in cholangiocarcinoma through genomic or genetic approaches, we expect that this orthotopic allograft mouse model will provide a powerful platform to investigate their impact on the initiation and maintenance of the disease.

Materials and Methods

Generation of Liver Carcinomas. All animal experiments were performed in accordance with a protocol approved by the Memorial Sloan–Kettering Institutional Animal Care and Use Committee. Isolation, culture, and retroviral transduction of fetal liver cells have been described previously (15, 16). Briefly, fetal liver cells were isolated by dispase digestion from developmental day14.5 mouse embryos, frozen, genotyped, and retrovirally transduced with MSCV-based vectors before orthotopic implantation. For subcapsular injection, the animals were anesthetized with isoflurane, and analgesia was provided by s.c. administration of buprenorphine directly before surgery. A subcostal transversal abdominal incision was performed and the left liver lobe was exposed. A total of $0.5–1 \times 10^6$ cells resuspended in 25 µL Matrigel were injected under the liver capsule using a Hamilton syringe and a 30-gauge needle. The injection site was sealed with Vetbond tissue adhesive (3M) and the abdominal wall was sutured using 4-0 Vicryl. The skin was closed with wound clips.

Doxycycline feed (625 mg/kg) purchased from Harlan Laboratories was replenished twice weekly. For orthotopic tumors, animals were killed when tumors reached a diameter of 10–15 mm as assessed by palpation or upon displaying signs of deterioration such as breathing failure or abdominal ascites. S.c. tumor volume was assessed by caliper measurements and calculated as $0.5 \times \text{length} \times \text{width}^2$ (length > width).

Derivation of Tumor Cell Lines. Tumors were isolated, mechanically dissociated with a scalpel, and subsequently enzymatically digested in DMEM supplemented with collagenase (2 mg/mL; Sigma C5138) and DNase I (4 units/mL; Ambion 2222) for 60 min at 37 °C in a shaking incubator (70 rpm). Crude digests were washed twice with PBS. For FACS, cells were stained with CD45-APC/Cy7 for 15 min at 4 °C after performing ACK lysis (5 min at room temperature). To generate cell lines, enzymatic digests were plated in DMEM supplemented with 10% (vol/vol) FBS and penicillin/streptomycin onto gelatin-coated cell culture dishes. Cells were enriched for epithelial tumor cells by differential trypsinization or by FACS sorting for GFP.

Statistical Analysis. Statistical analysis was performed using GraphPad Prism software by applying the log-rank (Mantel–Cox) test to compare survival data and the unpaired two-tailed t test for all other experimental data.

1. McLean L, Patel T (2006) Racial and ethnic variations in the epidemiology of intrahepatic cholangiocarcinoma in the United States. *Liver Int* 26(9):1047–1053.
2. Tyson GL, El-Serag HB (2011) Risk factors for cholangiocarcinoma. *Hepatology* 54(1):173–184.
3. Khan SA, et al.; British Society of Gastroenterology (2002) Guidelines for the diagnosis and treatment of cholangiocarcinoma: Consensus document. *Gut* 51(Suppl 6):VI1–VI9.
4. Endo I, et al. (2008) Intrahepatic cholangiocarcinoma: rising frequency, improved survival, and determinants of outcome after resection. *Ann Surg* 248(1):84–96.
5. Tannapfel A, et al. (2000) Mutations of p53 tumor suppressor gene, apoptosis, and proliferation in intrahepatic cholangiocellular carcinoma of the liver. *Dig Dis Sci* 45(2):317–324.
6. Ong CK, et al. (2012) Exome sequencing of liver fluke-associated cholangiocarcinoma. *Nat Genet* 44(6):690–693.
7. Tannapfel A, et al. (2003) Mutations of the BRAF gene in cholangiocarcinoma but not in hepatocellular carcinoma. *Gut* 52(5):706–712.
8. Tannapfel A, et al. (2000) Frequency of p16(INK4A) alterations and K-ras mutations in intrahepatic cholangiocarcinoma of the liver. *Gut* 47(5):721–727.
9. Gu TL, et al. (2011) Survey of tyrosine kinase signaling reveals ROS kinase fusions in human cholangiocarcinoma. *PLoS ONE* 6(1):e15640.
10. Benhamouche S, et al. (2010) Nf2/Merlin controls progenitor homeostasis and tumorigenesis in the liver. *Genes Dev* 24(16):1718–1730.
11. Sekiya S, Suzuki A (2012) Intrahepatic cholangiocarcinoma can arise from Notch-mediated conversion of hepatocytes. *J Clin Invest* 122(11):3914–3918.
12. Xu X, et al. (2006) Induction of intrahepatic cholangiocellular carcinoma by liver-specific disruption of Smad4 and Pten in mice. *J Clin Invest* 116(7):1843–1852.
13. Fan B, et al. (2012) Cholangiocarcinomas can originate from hepatocytes in mice. *J Clin Invest* 122(8):2911–2915.
14. O'Dell MR, et al. (2012) Kras(G12D) and p53 mutation cause primary intrahepatic cholangiocarcinoma. *Cancer Res* 72(6):1557–1567.
15. Zender L, et al. (2005) Generation and analysis of genetically defined liver carcinomas derived from bipotential liver progenitors. *Cold Spring Harb Symp Quant Biol* 70:251–261.
16. Zender L, et al. (2006) Identification and validation of oncogenes in liver cancer using an integrative oncogenomic approach. *Cell* 125(7):1253–1267.
17. Jonkers J, et al. (2001) Synergistic tumor suppressor activity of BRCA2 and p53 in a conditional mouse model for breast cancer. *Nat Genet* 29(4):418–425.
18. Olive KP, et al. (2004) Mutant p53 gain of function in two mouse models of Li-Fraumeni syndrome. *Cell* 119(6):847–860.
19. Postic C, et al. (1999) Dual roles for glucokinase in glucose homeostasis as determined by liver and pancreatic beta cell-specific gene knock-outs using Cre recombinase. *J Biol Chem* 274(1):305–315.
20. Postic C, Magnuson MA (2000) DNA excision in liver by an albumin-Cre transgene occurs progressively with age. *Genesis* 26(2):149–150.
21. Malato Y, et al. (2011) Fate tracing of mature hepatocytes in mouse liver homeostasis and regeneration. *J Clin Invest* 121(12):4850–4860.
22. Huang J, et al. (2012) Exome sequencing of hepatitis B virus-associated hepatocellular carcinoma. *Nat Genet* 44(10):1117–1121.
23. Jackson EL, et al. (2001) Analysis of lung tumor initiation and progression using conditional expression of oncogenic K-ras. *Genes Dev* 15(24):3243–3248.
24. Fellmann C, et al. (2011) Functional identification of optimized RNAi triggers using a massively parallel sensor assay. *Mol Cell* 41(6):733–746.
25. Schmitz KJ, et al. (2007) AKT and ERK1/2 signaling in intrahepatic cholangiocarcinoma. *World J Gastroenterol* 13(48):6470–6477.
26. Acquaviva J, Wong R, Charest A (2009) The multifaceted roles of the receptor tyrosine kinase ROS in development and cancer. *Biochim Biophys Acta* 1795(1):37–52.
27. Olive KP, et al. (2009) Inhibition of Hedgehog signaling enhances delivery of chemotherapy in a mouse model of pancreatic cancer. *Science* 324(5933):1457–1461.
28. Sawey ET, et al. (2011) Identification of a therapeutic strategy targeting amplified FGF19 in liver cancer by oncogenomic screening. *Cancer Cell* 19(3):347–358.
29. Scuoppo C, et al. (2012) A tumour suppressor network relying on the polyamine-hypusine axis. *Nature* 487(7406):244–248.
30. Zender L, et al. (2008) An oncogenomics-based in vivo RNAi screen identifies tumor suppressors in liver cancer. *Cell* 135(5):852–864.
31. Xue W, et al. (2007) Senescence and tumour clearance is triggered by p53 restoration in murine liver carcinomas. *Nature* 445(7128):656–660.
32. Holczbauer A, et al. (2013) Modeling pathogenesis of primary liver cancer in lineage-specific mouse cell types. *Gastroenterology* 145(1):221–231.
33. Sharma S, et al. (1989) Characterization of the ros1-gene products expressed in human glioblastoma cell lines. *Oncogene Res* 5(2):91–100.
34. Charest A, et al. (2003) Fusion of FIG to the receptor tyrosine kinase ROS in a glioblastoma with an interstitial del(6)(q21q21). *Genes Chromosomes Cancer* 37(1):58–71.
35. Bergethon K, et al. (2012) ROS1 rearrangements define a unique molecular class of lung cancers. *J Clin Oncol* 30(8):863–870.